Electronic Supplementary Information

Promoting effect of amorphous support on ruthenium-based catalyst for electrochemical hydrogen evolution reaction

Zhandong Ren,‡* Miaojie Tian,‡ Ning Cong, Hucheng Jiang, Hongwei Jiang, Zhiqiang Xie, Juanjuan Han and Yuchan Zhu*

School of Chemical and Environmental Engineering, Wuhan Polytechnic University, Wuhan, 430023, P. R. China.

‡ Z. Ren and M. Tian contributed equally to this work.

* Corresponding author:

Zhandong Ren, Professor, School of Chemical and Environmental Engineering, Wuhan Polytechnic University, Wuhan, 430023, P. R. China.

E-mail: renzhandong@163.com. Tel.: 86-27-83943956.

Yuchan Zhu, Professor, School of Chemical and Environmental Engineering, Wuhan Polytechnic University, Wuhan, 430023, P. R. China.

E-mail: zhuyuchan@163.com. Tel.: 86-27-83943956.

1. Experimental methods

1.1 Chemicals and materials

Cobalt target (Co ≥ 99.99%) was purchased from Beijing Goodwill Metal Technology Development Co. Ltd. Commercial Pt/C (40% loading, 2-5 nm Pt size is Johnson Matthey Co. Ltd. Ruthenium trichloride ($RuCl_3 \cdot 3H_2O$, AR), acetone (CH_3COCH_3, AR), ethanol (C_2H_5OH, AR), potassium hydroxide (KOH, AR), titanium foil (Ti, 99.99%) and cobalt foil (Co, 99.99%) were purchased from Sinopharm Chemical Reagent Co. Ltd., Shanghai, China. All reagents were analytical grade and used without further purification. Argon gas (99.999%) was purchased from Ming-Hui Company. The water (18.25 MΩ cm^{-1}) used in all experiments was prepared by passing through an ultra-pure purification system.

1.2 Preparation of a-Co/Ti

Using Co disk (99.9%) as sputtering target and Ti foil (99.9%) as substrate, amorphous Co nanosheet (a-Co/Ti) was prepared in high vacuum magnetron sputtering instrument (TRP-450, SKY Technology Development, China). The detailed process of the experiment is as follows. A 2 mm thick Co target was mounted on a sputtering target base with a strong magnetic field. The matrix is a Ti foil, which is ultrasonically cleaned by acetone, water and ethanol and then transferred into a vacuum chamber. Before sputtering, the vacuum chamber was evacuated to 5×10^{-4} Pa to ensure the removal of impurity gases such as oxygen. Then high purity argon (99.999%) was introduced to adjust the pressure in the vacuum chamber to 1.0 Pa. The purpose of introducing high purity argon is to produce Ar^+ by ionization. Co target was controlled by DC power supply with 100 W. During sputtering, a DC power supply is used for ionization, and a negative bias voltage is applied to the cathode target, so that Ar gas is ionized into Ar^+ ions. The Ar^+ ions generated in the discharge process are accelerated to bombard the Co target surface (cathode target), and cause Co atoms to become sputtering atoms. When sputtered Co atoms reach the surface of Ti substrate, their initial positions are random and disordered. The rapid migration and uniform diffusion of Co atoms

adsorbed on the Ti substrate can be promoted by adjusting the Ti substrate temperature.

1.3 Preparation of ld-Ru@a-Co/Ti and Ru@c-Co

The ld-Ru@a-Co/Ti is prepared through the hydrothermal ion exchange using a-Co/Ti as a "template". Put the a-Co/Ti or Co foil into the bottom of the inner liner of the autoclave. Then accurately pipet 30 mL of 0.2 mmol L^{-1} $RuCl_3$ solution ($V_{ethanol}$: $V_{isopropanol}$ = 1:1) and add it to the inner container of the autoclave without adding any surfactant. Then the hydrothermal reaction was carried out at 180°C for 6h. After the reaction, the samples were dried in vacuum at 60°C for 1 h and named ld-Ru@a-Co/Ti and Ru@c-Co respectively. The total loading of Ru and Co of ld-Ru@a-Co/Ti is about 24 μg cm^{-2}. The loading of Ru of Ru@c-Co is about 24 μg cm^{-2}.

1.4 Preparation of 50 wt% Ru/C electrode

0.2449g $CH_3COONa·3H_2O$ was dissolved with a small amount of water, and then 30 mL of 0.2 mmol L^{-1} $RuCl_3$ solution ($V_{ethanol}$: $V_{isopropanol}$ = 1:1) was added, which was uniformly mixed after ultrasonic dispersion for 10 min, and then added into the inner container of the autoclave. The hydrothermal reaction temperature was set at 180℃ and the time was set at 6h. When the hydrothermal reaction is finished, the samples are washed with absolute ethyl alcohol and ultrapure water respectively, and dried in vacuum at 60℃ for 1h to get Ru power. Ru powder and C powder were mixed according to the weight ratio of 1:1, and wet milled for 5 h in the presence of a small amount of ethanol, so that they were fully mixed to obtain Ru/C sample after vacuum drying. 1 mg of 50 wt% Ru/C sample was added to 1 ml of 0.05 wt% nafion-ethanol solution, and dispersed uniformly by ultrasound. 24 μL of catalyst ink was evenly dripped on a Ti foil to prepare a 50 wt% Ru/C electrode. The loading of Ru is about 24 μg cm^{-2}.

1.5 Preparation of 40 wt% Pt/C electrode

Add 1 mg of commercial 40 wt% Pt/C sample to 1 mL of 0.05 wt% nafion-ethanol solution, and ultrasonically disperse uniformly. Pipette 30 μL of catalyst ink droplets

on a Ti foil with an electrode area of 0.5 cm^2 to prepare a 40wt% Pt/C electrode. The loading of Pt is about 24 μg cm^{-2}.

1.6 Material characterization

X-ray diffraction (XRD) patterns were acquired on an XRD-7000 X-ray diffractometer (Shimadzu, Japan). Transmission Electron Microscopy (TEM) were conducted on an JEM-2100F (JEOL, Japan). Scanning Electron Microscope (SEM) images were taken with a ΣIGMA field-emission SEM (Zeiss, Germany). X-ray photoelectron spectrometry (XPS: ESCLAB 250Xi, Thermo Fisher Scientific, The United States) with monochromatized Al Ka radiation was used to analyze the electronic properties. Analysis of the composition of the electrode was carried out by X-ray fluorescence (XRF: EDX-7000, Shimadzu, Japan).

1.7 Electrochemical measurements

The electrochemical experiments were carried out in a typical three-electrode electrochemical cell with a carbon paper as a counter electrode (TGP-H-090, Toray, Japan) and Hg/HgO/KOH (1.0 M) as the reference electrode (R0501, Tianjin Aida Hengsheng Technology Development Co., Ltd, China). Cyclic voltammetry (CV) measurements were performed in Ar-saturated 1.0 M KOH solution at the scan rate of 100 mV s^{-1}. The electrochemical surface areas (ECSAs) were calculated by scanning the double layer (0.826-0.926 V vs. RHE) at different scanning rates (10, 20, 40, 50, 60, 70, 80, 100 mV s^{-1}). The C_{dl} can be obtained by linearly fitting the double-layer current to the scan rate. Further divide the C_{dl} by the capacitance constant (C_{ref}, 60 mC cm^{-2}) to obtain ECSA. The HER activity was characterized by linear voltammetry scanning (LSV) in 1.0M KOH solutions at a scanning speed of 5 mV s^{-1} with 80% IR correction. Electrochemical impedance spectroscopy (EIS) was recorded under the condition of overpotential of 20 mV, frequency of 100 mHz ~ 100 kHz and ac voltage amplitude of 10 mV. The accelerated life test of the electrode was conducted for 10 h by the chronoamperometry method. The overall water splitting experiment was a two-electrode system with ld-Ru@a-Co/Ti electrode as cathode and RuO_2/Ti electrode as

anode (denoted as (-) ld-Ru@a-Co/Ti // RuO_2/Ti (+)) in 1.0 M KOH solution. The overall water splitting stability experiment was carried out for 12 h.

1.8 Tafel analysis of HER mechanism

The Tafel slope of ld-Ru@a-Co/Ti is only 39.6 mV dec^{-1}. The Tafel slope of ld-Ru@a-Co/Ti can prove that the reaction processes is the Volmer-Heyrovsky mechanism.

In alkaline solutions, the mechanism of HER mainly involves three reactions (eqn (1)–(3)).

The discharge reaction (Volmer step) is:

$$H_2O + e^- \rightarrow H_{ad} + OH^-$$

$$b = 2.303RT/\alpha F = 116\ mV.dec^{-1} \quad \alpha = 0.5 \qquad (1)$$

The combination reaction (Tafel step) is:

$$H_{ad} + H_{ad} \rightarrow H_2$$

$$b = 2.303RT/2F = 29\ mV.dec^{-1} \qquad (2)$$

The ion + atom reaction (Heyrovsky step) is:

$$H_2O + H_{ad} + e^- \rightarrow H_2 + OH^-$$

$$b = 2.303RT/[(1+\alpha)F] = 38mV.dec^{-1} \quad \alpha = 0.5 \qquad (3)$$

Commonly, the HER mechanism can be determined by the Tafel slope of different catalysts. The mechanism of hydrogen evolution kinetics had been discussed in the article by Bockris (J. Electrochem. Soc. 1952, 99, 169). Assuming a small surface coverage of hydrogen, a fast discharge reaction (1) followed by a rate-determining combination reaction (2) results in a theoretical Tafel slope of 29 mV·dec^{-1} (2.303RT/2F) at 25℃. If the electrochemical desorption step (3) is rate-determining step, the Tafel slope is 38 mV·dec^{-1} (2.303RT/1.5F) at 25℃. If reaction (2) is rate determining or the surface coverage is close to one, the Tafel slope should be 116 mV·dec^{-1}.

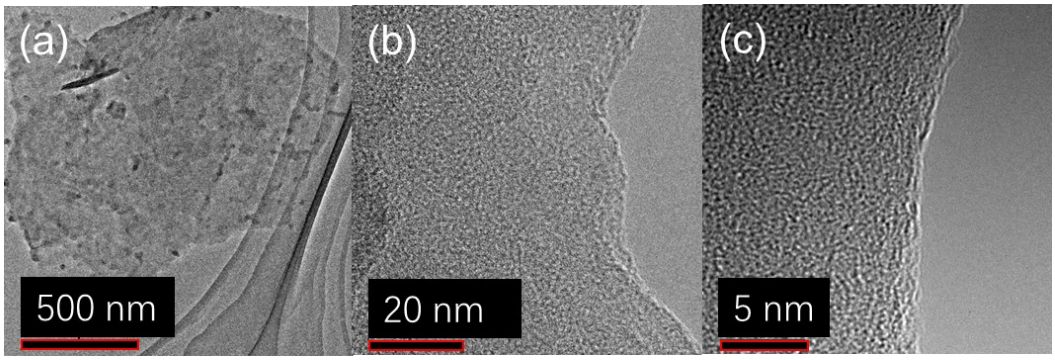

Figure S1 TEM images of a-Co/Ti.

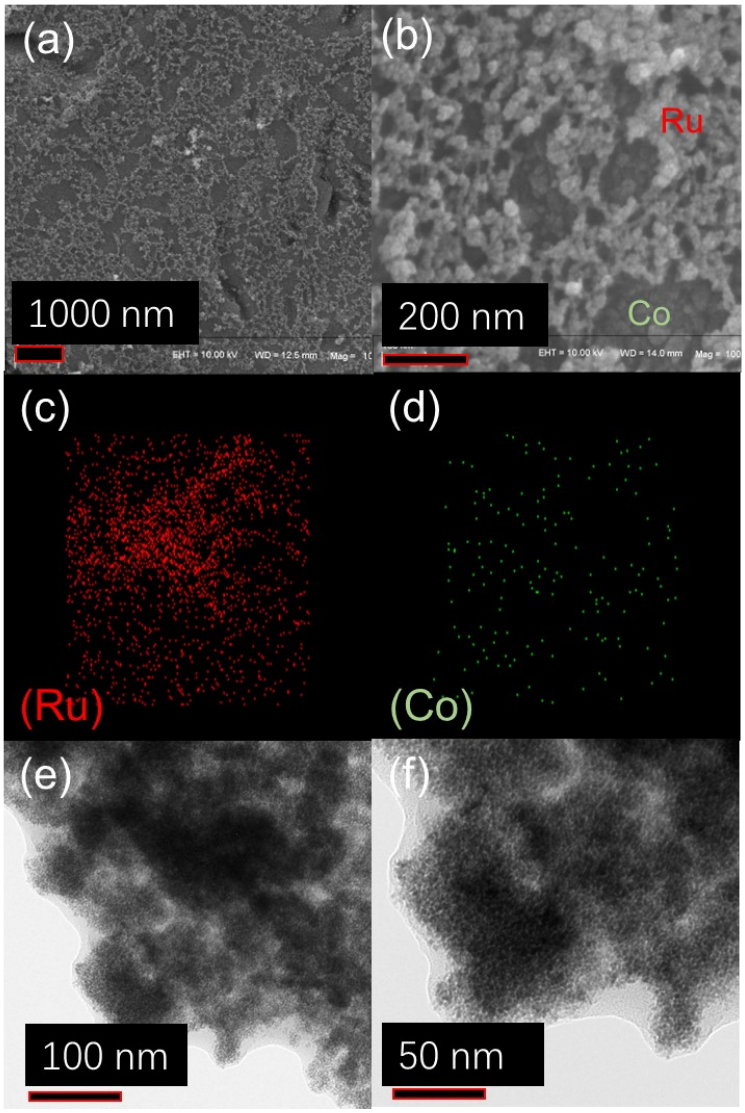

Figure S2 SEM images (a-b), EDS mappings (c-d) and TEM images (e-f) of ld-Ru@a-Co/Ti.

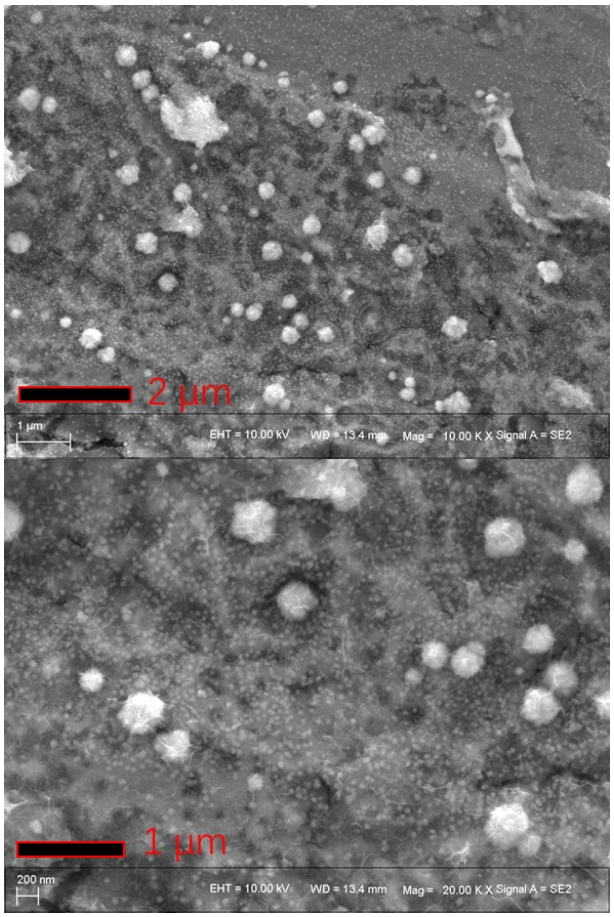

Figure S3 SEM images of Ru@c-Co prepared by hydrothermal method with Co foil substrate.

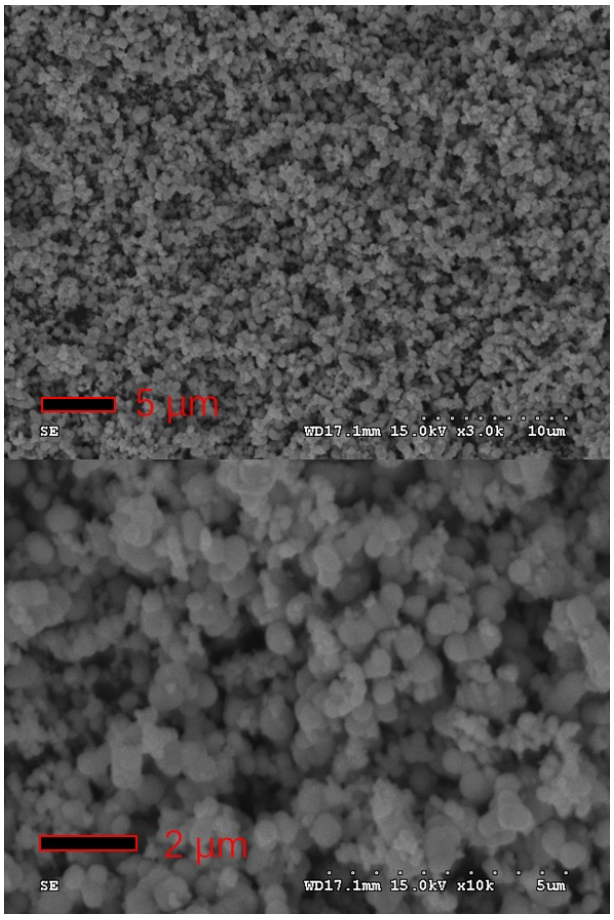

Figure S4 SEM images of Ru prepared by hydrothermal method without the substrate.

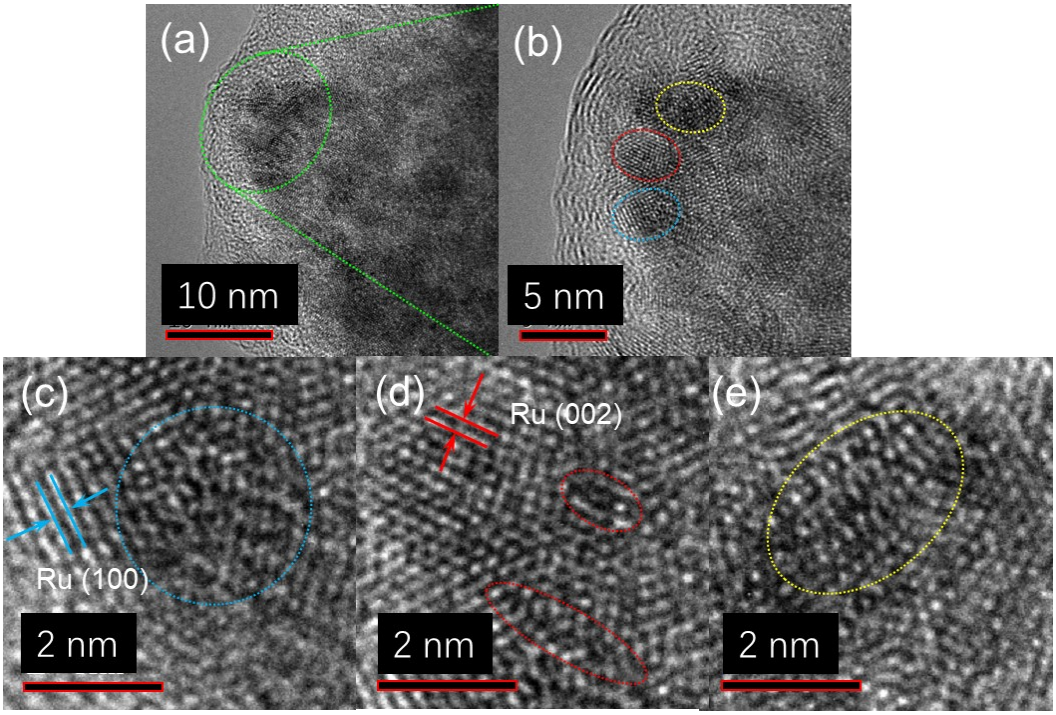

Figure S5 The lattice defects of ld-Ru@a-Co/Ti with HRTEM investigation.

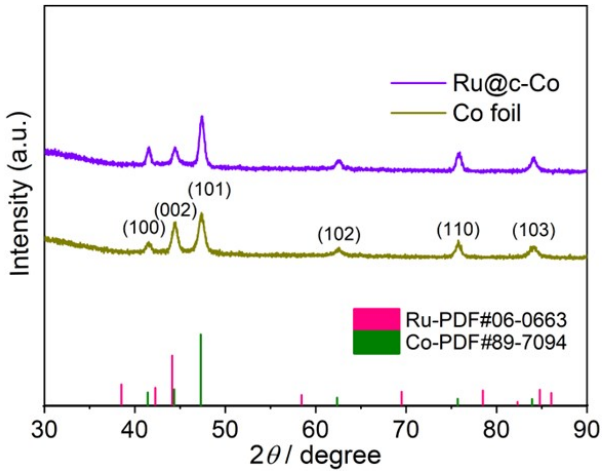

Figure S6 The XRD patterns of Co foil and Ru@c-Co.

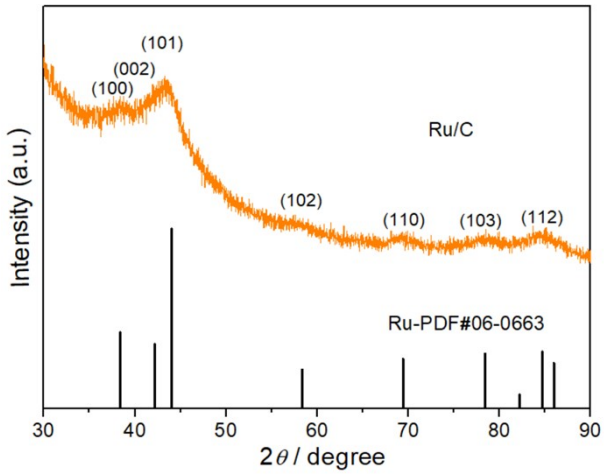

Figure S7 The XRD patterns of Ru prepared by hydrothermal method without the substrate.

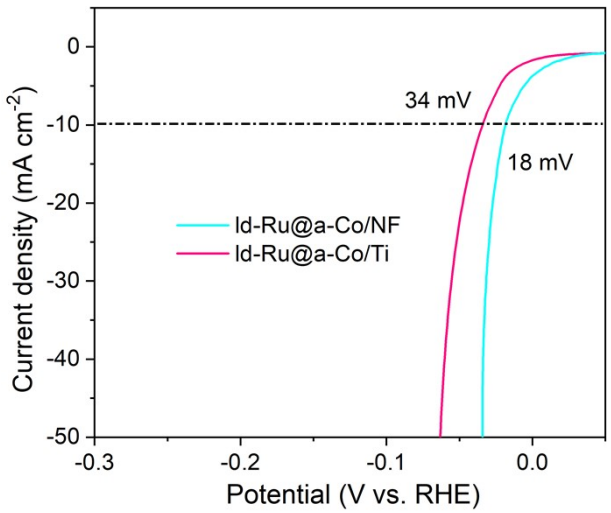

Figure S8 The Linear sweep voltammetry (LSV) curves of ld-Ru@a-Co/Ti and ld-Ru@a-Co/NF.

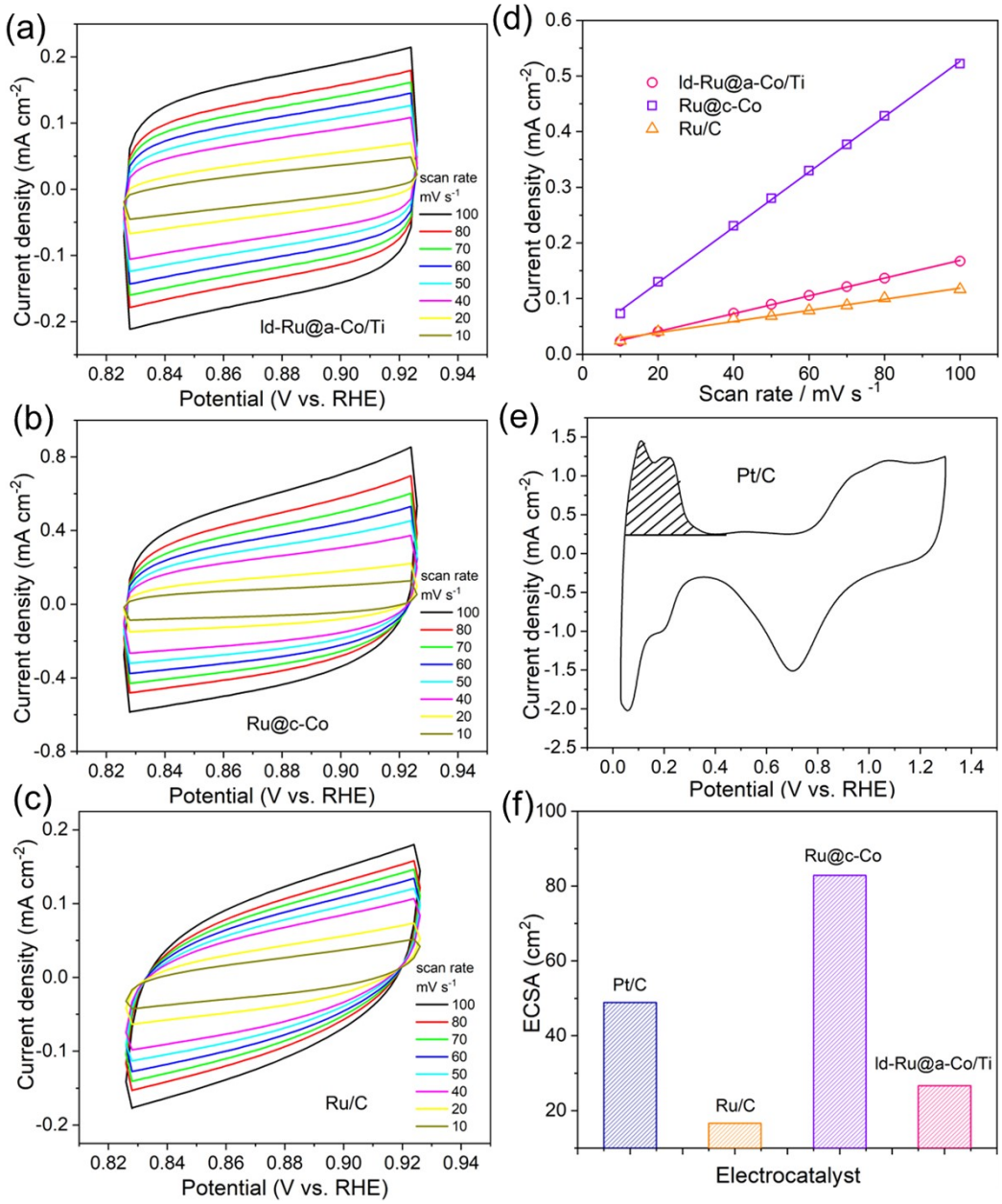

Figure S9 The double layer current at different scanning speeds of ld-Ru@a-Co/Ti (a), Ru@c-Co (b) and Ru/C (c). The double-layer capacitance (C_{dl}) of ld-Ru@a-Co/Ti, Ru@c-Co and Ru/C (d). The cyclic voltammogram (CV) of Pt/C (e). The electrochemical surface areas (ECSAs) of ld-Ru@a-Co/Ti, Ru@c-Co, Ru/C and Pt/C (f).

The ECSAs of three Ru catalysts are gained using double-layer capacitance (C_{dl}) (Fig. S9 a-c). The C_{dl} of Ru/C is 1.00 mF cm^{-2}, while the C_{dl} of ld-Ru@a-Co/Ti and Ru@c-Co are 1.60 and 4.97 mF cm^{-2} in Fig. S9d. The ECSAs of Ru/C, ld-Ru@a-Co/Ti and Ru@c-Co are 16.66, 26.67 and 82.83 cm^2 in Fig. S9f. The ECSA of Pt/C catalyst is obtained from the charge of underpotential deposition of H in cyclic voltammetry (CV) (Fig. S9 e). The ECSA of Pt catalyst is 48.89 cm^2 in Fig. S9f.

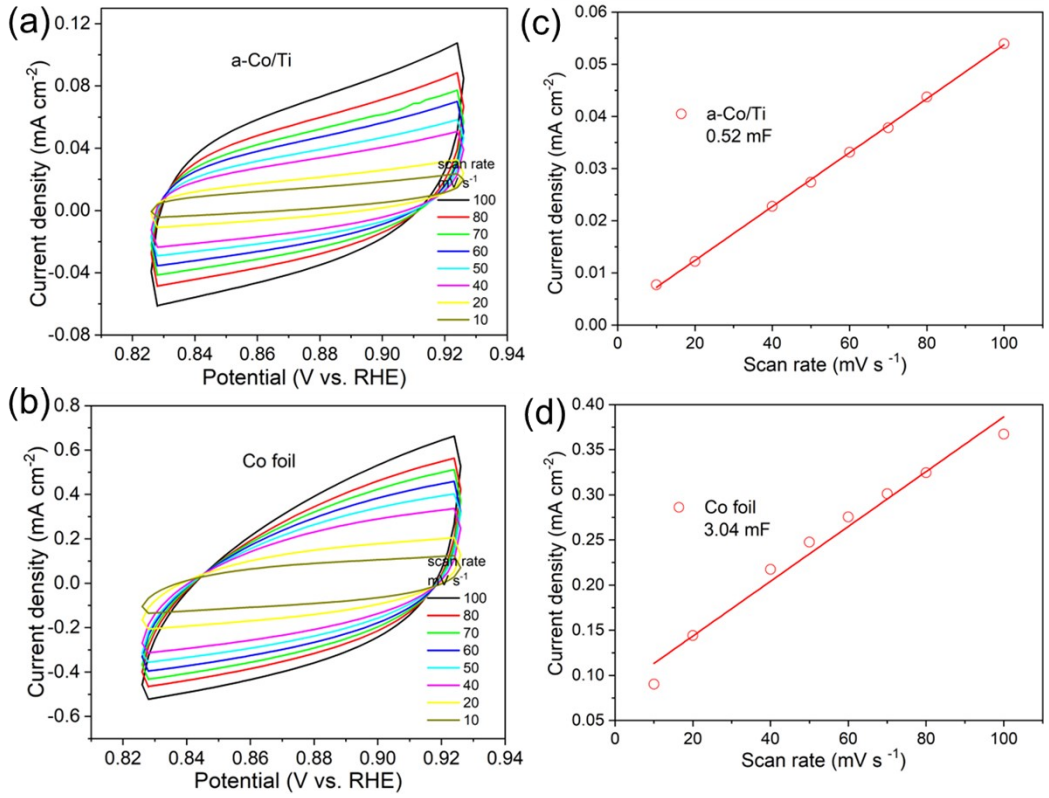

Figure S10 The double layer current at different scanning speeds of a-Co/Ti (a) and Co foil (b). The double-layer capacitance (C_{dl}) of a-Co/Ti (c) and Co foil (d).

The C_{dl} of three types of Ru catalysts are shown in Fig. S9e. Among them, the C_{dl} of Ru/C is 1.00 mF cm^{-2}, while the C_{dl} of ld-Ru@a-Co/Ti and Ru@c-Co are 1.60 and 4.97 mF cm^{-2}. The C_{dl} of ld-Ru@a-Co/Ti and Ru@c-Co both exceed that of Ru/C, which may be caused by the C_{dl} of their own Co matrix. Therefore, the C_{dl} of a-Co/Ti and Co foil are further tested in Fig. S10, which are 0.52 and 3.04 mF cm^{-2}. Then, if the influence of Co matrix on C_{dl} is deducted, the ECSA of the three types of Ru-based catalysts has little difference. The ECSA of Ru/C is 16.66 cm^2, while the ECSAs of ld-Ru@a-Co/Ti and Ru@c-Co are 18.00 and 32.17 cm^2. The sequence of ECSA is inconsistent with the sequence of HER activity, so it is not the main reason for increasing HER activity.

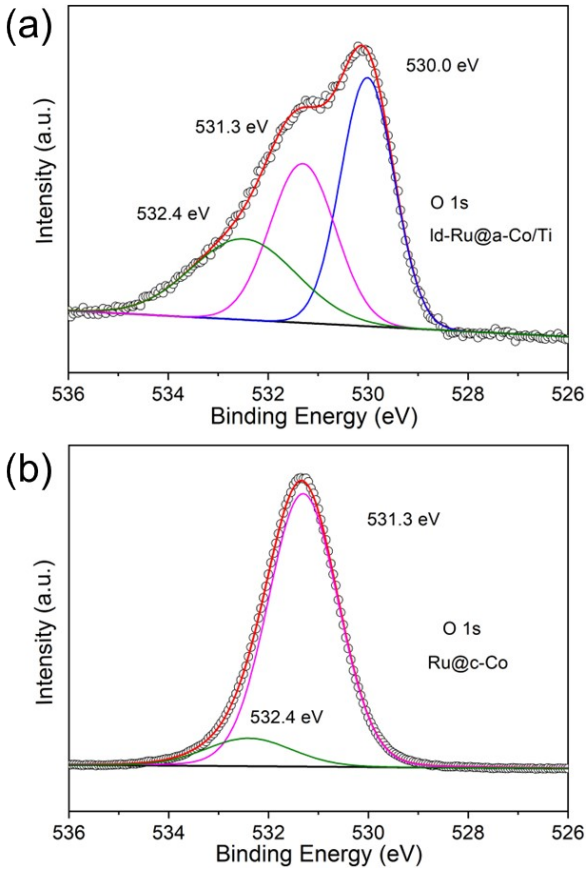

Figure S11 The XPS of O 1s in the ld-Ru@a-Co/Ti (a) and Ru@c-Co (b).

There are three forms of adsorbed oxygen in the O1s peaks of ld-Ru@a-Co/Ti, namely O^{2-} (530.0 eV), OH^- (531.3 eV) and H_2O (532.5 eV). However, for the Ru@c-Co, there are only two adsorbed oxygens, namely OH^- (531.3 eV) and H_2O (532.4 eV). This indicates that the surface of ld-Ru@a-Co/Ti has abundant oxidation states, which is due to the amorphous structure of Co and lattice defects of Ru.

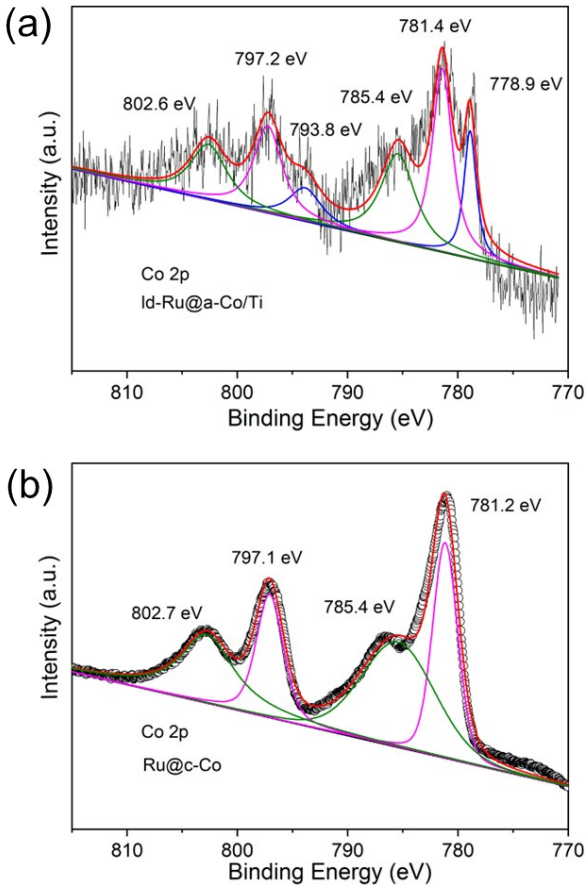

Figure S12 The XPS of Co 2p in the ld-Ru@a-Co/Ti (a) and Ru@c-Co (b)

For the Co 2p orbital, the Co^{2+} and Co^{4+} spin-orbit splitting peaks can be observed at 781.4, 797.2 and785.4, 802.6 eV for ld-Ru@a-Co/Ti and the Co^{2+} and Co^{4+} spin-orbit splitting peaks can be observed at 781.2, 797.1 and785.4, 802.7 eV for Ru@c-Co.

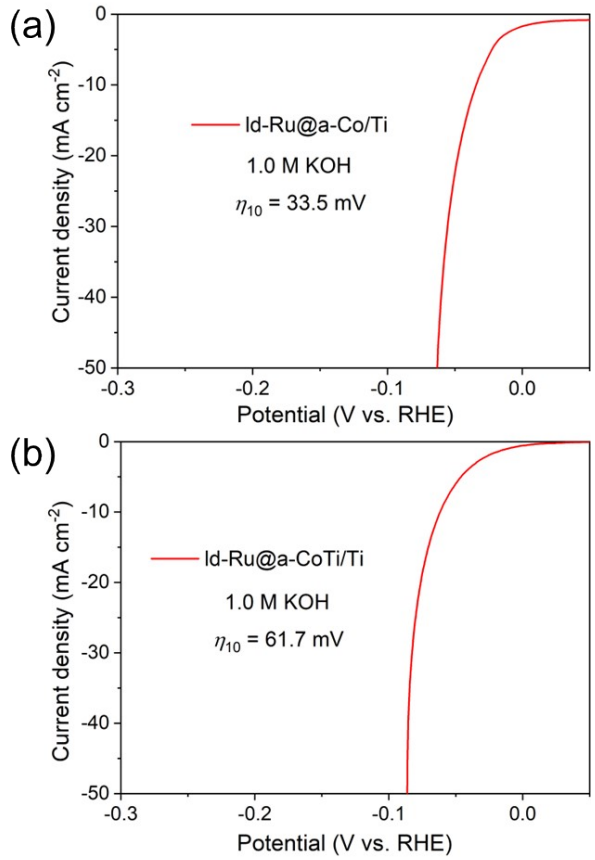

Figure S13 The HER activities of ld-Ru@a-Co/Ti (a) and ld-Ru@a-CoTi/Ti (b).

In order to prove whether the Ti matrix can improve the performance of HER, the CoTi/Ti support is prepared by the cosputtering Co and Ti (Co:Ti = 9:1). And then the ld-Ru@a-CoTi/Ti is obtained by the modification of trace Ru in the subsequent hydrothermal ion exchange. The HER activity of the ld-Ru@a-CoTi/Ti is compared with that of the ld-Ru@a-Co/Ti in Fig. S13. The HER activity of the ld-Ru@a-CoTi/Ti (η_{10} = 61.7 mV) is obviously worse than that of the ld-Ru@a-Co/Ti (η_{10} = 33.5 mV), which preliminarily indicates that Ti has no promoting effect on the HER activity of the ld-Ru@a-Co/Ti.

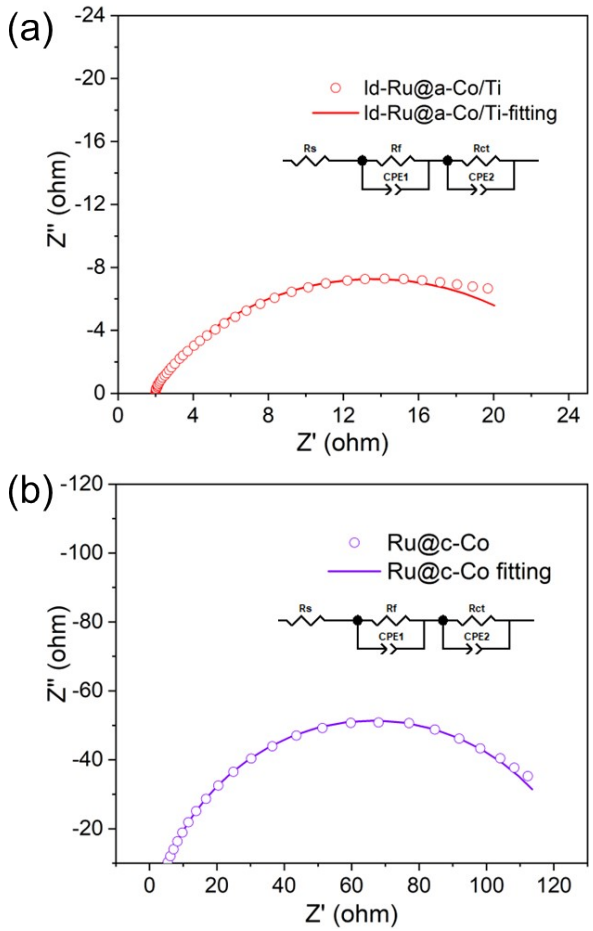

Figure S14 The EIS measurements of the ld-Ru@a-Co/Ti (a) and Ru@c-Co (b) at η = 20 mV.

Fig. S14 a and b are the Nyquist plots of Ru@c-Co and ld-Ru@a-Co/Ti at -0.02 V. The equivalent circuit is fitted by Zview software ($R_s(R_fC_f)(R_{ct}C_{dl})$). The solution resistance (R_s) of Ru@c-Co and ld-Ru@a-Co/Ti electrodes is almost the same, which is 1.88 and 2.26 Ω cm^2, respectively. However, for the charge transfer resistance (R_{ct}), the R_{ct} of ld-Ru@a-Co/Ti (23.46 Ω cm^2) is obviously lower than that of Ru@c-Co (128.2 Ω cm^2). The low R_{ct} of ld-Ru@a-Co/Ti indicates that its charge transfer is fast in HER process.

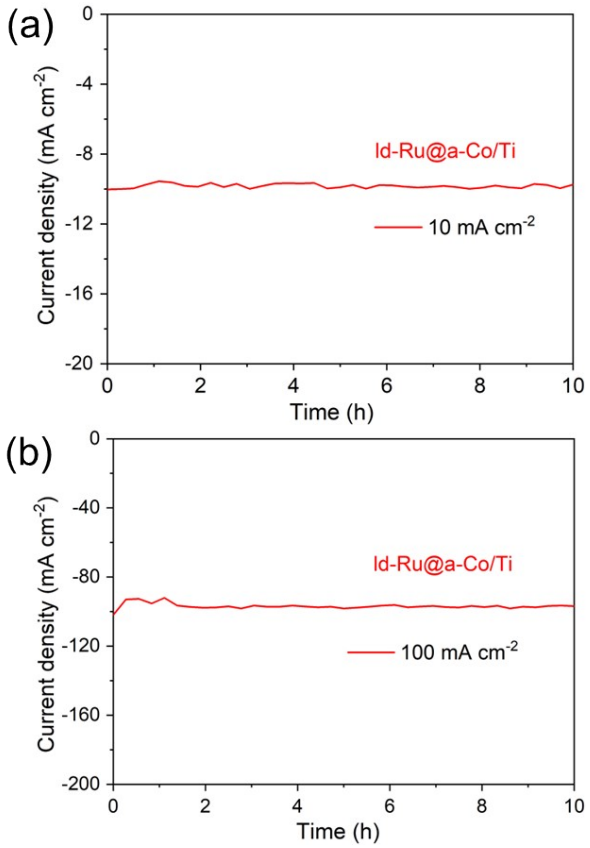

Figure S15 Accelerated life test of the ld-Ru@a-Co/Ti in the HER process with the initial current density of 10 (a) and 100 (b) mA cm^{-2}.

The accelerated life test of the ld-Ru@a-Co/Ti electrode in the HER process is shown in Fig. S15, and the result shows that the HER activity remains unchanged after the 10 h of chronoamperometry testing.

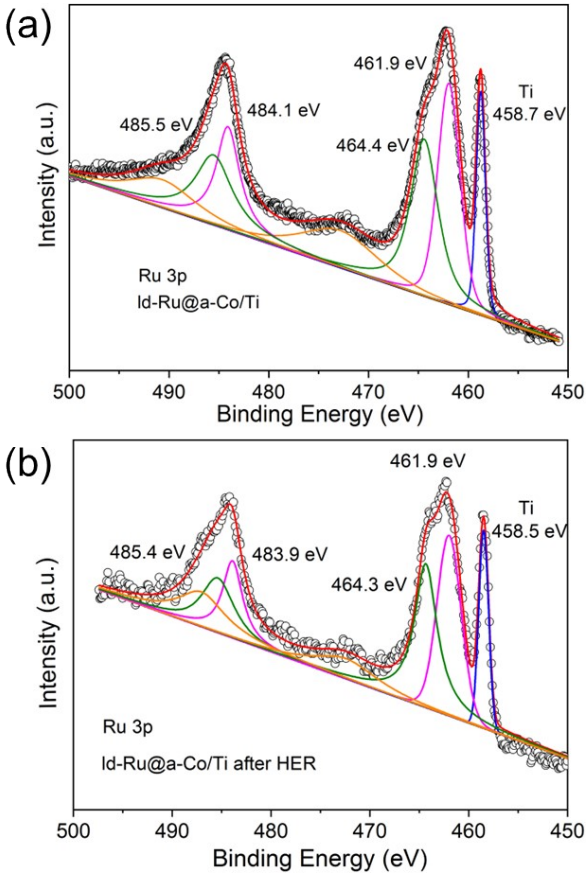

Figure S16 XPS spectra of the ld-Ru@a-Co/Ti before (a) and after (b) the accelerated life test.

The XPS characterization of ld-Ru@a-Co/Ti electrode after the accelerated life test indicates that the B.E. peak positions and valence states have no obvious change. This further illustrates the excellent stability of ld-Ru@a-Co/Ti electrode.

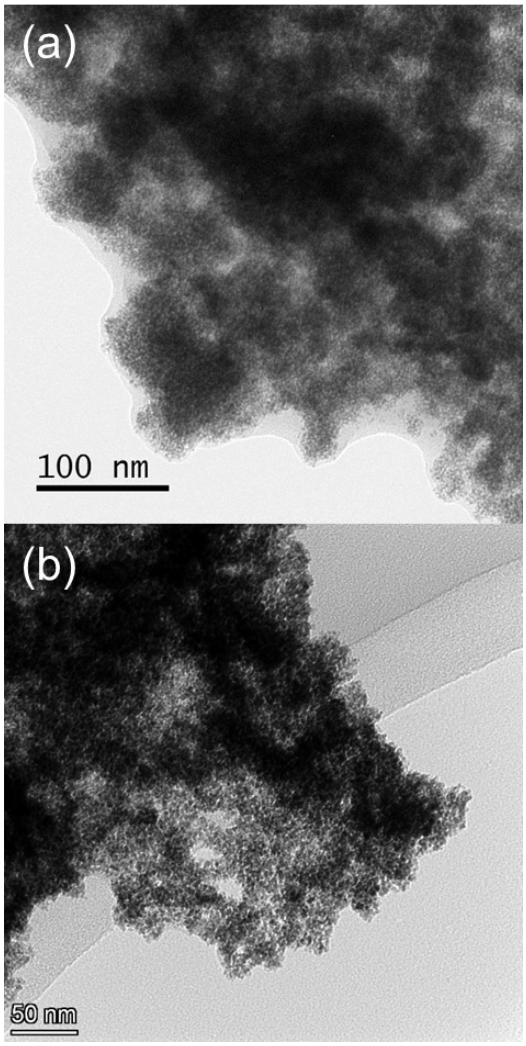

Figure S17 TEM images of the ld-Ru@a-Co/Ti before (a) and after (b) the accelerated life test.

The TEM characterization of the ld-Ru@a-Co/Ti electrode after the accelerated life test indicates that its morphology has not changed significantly, and there is no agglomeration phenomenon.

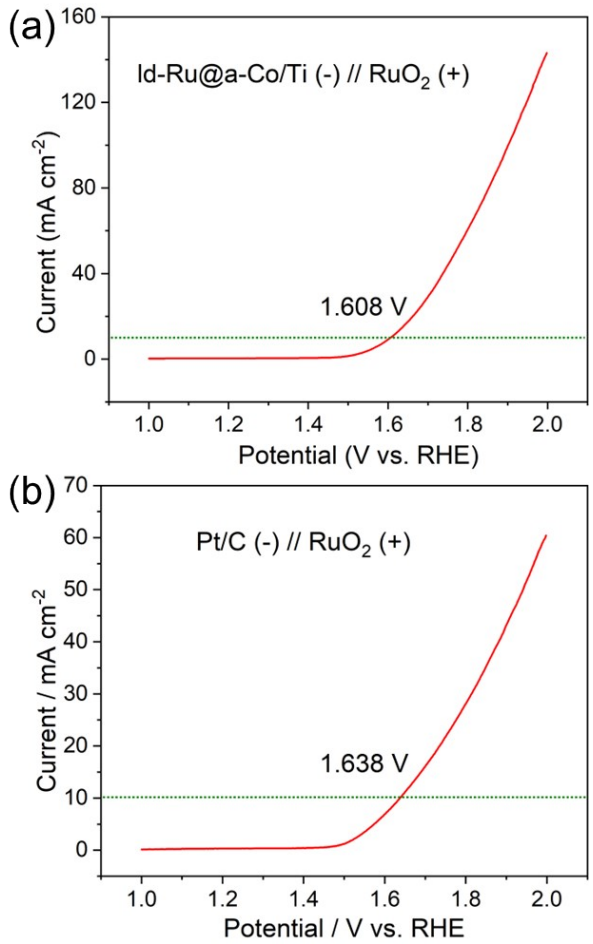

Figure S18 The overall water splitting capabilities of (-) ld-Ru@a-Co/Ti // RuO_2/Ti (+) (a) and (-) Pt/C/Ti // RuO_2/Ti (+) in 1.0 M KOH solution (b).

Further, in order to verify the overall water splitting capability, a two-electrode system with ld-Ru@a-Co/Ti electrode (23.9 μg cm^{-2}) as cathode and RuO_2/Ti electrode (24 μg cm^{-2}) as anode (denoted as (-) ld-Ru@a-Co/Ti // RuO_2/Ti (+)) was constructed in 1.0 M KOH solution. A comparative evaluation of (-) Pt/C/Ti // RuO_2/Ti (+) water electrolyzer composed of Pt/C (cathode) (24 μg cm^{-2}) and RuO_2 (anode) (24 μg cm^{-2}) was carried out. The recorded polarization curves indicate that the (-) ld-Ru@a-Co/Ti // RuO_2/Ti (+) cell needs a lower voltage of 1.608 V to achieve 10 mA cm^{-2} in Fig. S18a, which is obviously lower than the 1.638 V required by (-) Pt/C/Ti // RuO_2/Ti (+) cell in Fig. S18b. It should be noted that the voltage of water decomposition in this paper does not show obvious advantages compared with those of other literatures, which may be due to the extremely low electrode loading (whether cathode or anode) in this study.

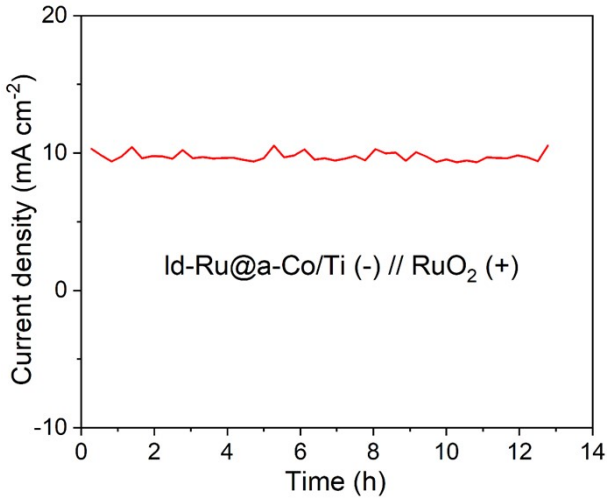

Figure S19 The overall water splitting stability of (-) ld-Ru@a-Co/Ti // RuO_2/Ti (+) in 1.0 M KOH solution.

In addition, in Fig. S19, for (-) ld-Ru@a-Co/Ti // RuO_2/Ti (+) cell, it can be well maintained at a constant current density of 10 mA cm^{-2} for 12 h.

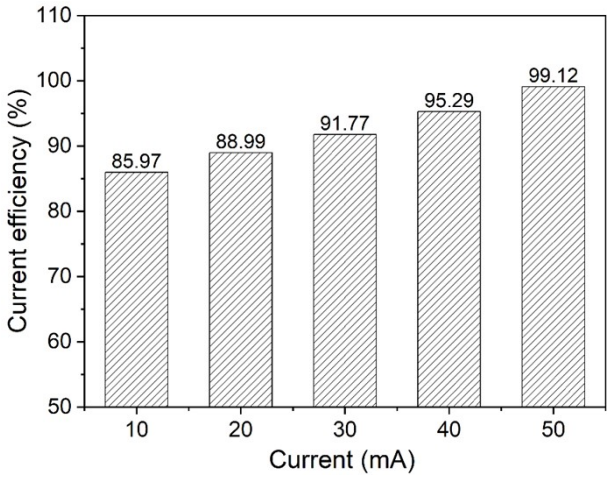

Figure S20 The faradic efficiencies of the ld-Ru@a-Co/Ti under different currents.

The faradic efficiency of ld-Ru@a-Co/Ti electrocatalyst have been supplied to confirm the efficiency for hydrogen evolution. When the current is in the range of 10 ~ 50 mA, the faradic efficiency of ld-Ru@a-Co/Ti is in the range of 85.97 ~ 99.12 %, which indicates that the hydrogen evolution efficiency is high.

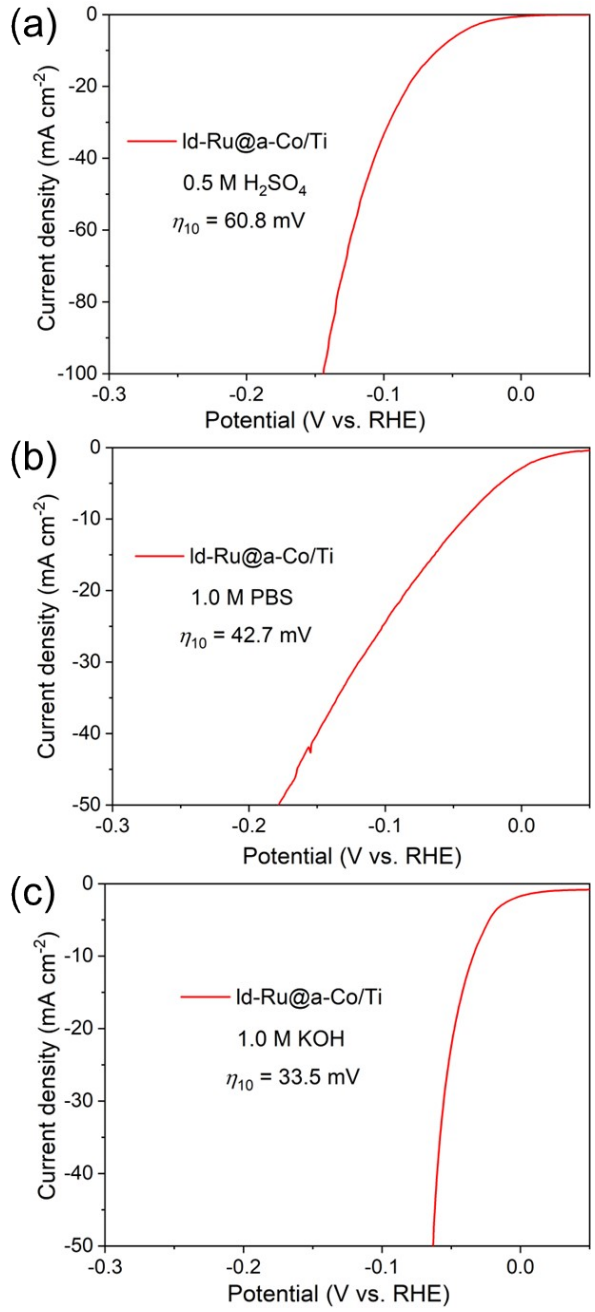

Figure S21 The HER activities of the ld-Ru@a-Co/Ti in 0.5 M H_2SO4,(a) 1.0 M PBS (pH = 7) (b) and 1.0 M KOH (c) solutions.

The comparison of HER activities of the ld-Ru@a-Co/Ti in acidic, neutral and alkaline solutions have been added in Fig. S21. The η_{10} of ld-Ru@a-Co/Ti electrode is 60.8, 42.7 and 33.5 mV in 0.5 M H_2SO_4, 1.0 M PBS and 1.0 M KOH, respectively. The above results can demonstrate that the ld-Ru@a-Co/Ti has an excellent HER activity in a wide pH range.

Table S1. Comparison of HER activities in 1.0 M KOH between optimized ld-Ru@a-Co/Ti and other Ru-based electrocatalysts in literatures.

Catalyst	**Total Loading ($\mu g\ cm^{-2}$)**	**η_{10} (mV)**	**Tafel slope $mV\ dec^{-1}$**	**References**
Ru1/D-NiFe LDHs	2000	18	29	**(1)**
Ru-a-CoNi	1800	15	34	**(2)**
Ru@Ni-MOF	1200	22	40	**(3)**
Ru-MoS_2/CNT	1000	50	62	**(4)**
RuSA–N-$Ti_3C_2T_x$	1000	27	29	**(5)**
RuNi/CFC	770	43	--	**(6)**
Ru@Co-NC	764	23	58.1	**(7)**
Ru-NiCo-LDH	700	28	--	**(8)**
Ru NP/C	590	24	33	**(9)**
Ru/H–S,N–C	350	32	24	**(10)**
Ru-CN/MC	340	17	38	**(11)**
RuCo NPs/CNTs	306	27	27	**(12)**
$RuSe_2$	300	34	95	**(13)**
Ru@CNF	300	19.6	23.8	**(14)**
SA-Ru-MoS_2	285	76	21	**(15)**
RuPx/C	285	31	31.1	**(16)**
$RuRh_2$	286	24	31	**(17)**
Ru@NCN	260	36	33	**(18)**
RuCo@NC-600	255	34	36	**(19)**
MoRu	254	27	51	**(20)**
Ru-Mo_2C/CN	250	34	80	**(21)**
Ru/C_3N_4/C	204.8	79	--	**(22)**
Ru/C-TiO_2	200	44	73.7	**(23)**
Ru-Mo_2C@CNT	143	15	26	**(24)**
Ru-MoO_2@PC/rGO	140	126	43.5	**(25)**
Ru@Co/N-CNTs	125	48	33	**(26)**
ld-Ru@a-Co/Ti	23.9	34	62	This work
ld-Ru@a-Co/NF	23.9	18	29	This work

References

1. P. Zhai, M. Xia, Y. Wu, G. Zhang, J. Gao, B. Zhang, S. Cao, Y. Zhang, Z. Li, Z. Fan, C. Wang, X. Zhang, J. T. Miller, L. Sun and J. Hou. *Nat. Commun.*, 2021, **12**, 4587.
2. Y. Liu, X. Liu, A. R. Jadhav, T. Yang, Y. Hwang, H. Wang, L. Wang, Y. Luo, A. Kumar, J. Lee, H. T. D. Bui, M. G. Kim and H. Lee. *Angew. Chem. Int. Ed.*, 2022, **61**, e202114160.
3. L. Deng, F. Hu, M. Ma, S.-C. Huang, Y. Xiong, H.-Y. Chen, L. Li, and S. Peng. *Angew. Chem. Int. Ed.*, 2021, **60**, 1-8.
4. X. Zhang, F. Zhou, S. Zhang, Y. Liang, and R. Wang, *Adv. Sci.*, 2019, **6**, 1900090.

5. H. Liu, Z. Hu, Q. Liu, P. Sun, Y. Wang, S. Chou, Z. Hu and Z. Zhang, *J. Mater. Chem. A*, 2020, **8**, 24710-24717.
6. M. Yuan, C. Wang, Y. Wang, Y. Wang, X. Wang and Y. Du. *Nanoscale*, 2021, **13**, 13042–13047.
7. H. Gao, J. Zang, X. Liu, Y. Wang, P. Tian, S. Zhou, S. Song, P. Chen and W. Li, *Appl. Surf. Sci.*, 2019, **494**, 101-110.
8. D. Li, B. Zhang, Y. Li, R. Chen, S. Hu and H. Ni, *Electrochem. Commun.*, 2019, **101**, 23-27.
9. Q. Wang, M. Ming, S. Niu, Y. Zhang, G. Fan and J.-S. Hu, *Adv. Energy Mater.*, 2018, **8**, 1801698.
10. Y. Wang, W. Luo, H. Li and C. Cheng, *Nanoscale Adv.*, 2021, **3**, 5068–5074.
11. X. Liu, T. L. Jin, Z. D. Hood, C. Tian, Y. Guo and W. Zhan, *ChemElectroChem*, 2019, **6**, 2719-2725.
12. B. Zhang, P. Zhao and T. Wu, *ACS Appl. Energy Mater.*, 2022, **5**, 5633−5643.
13. Y. Zhao, H. Cong, P. Li, D. Wu, S. Chen and W. Luo, *Angew. Chem. Int. Ed.*, 2020, **60**, 7013-7017.
14. Q. Xie, Z. Wang, L. Lin, Y. Shu, J. Zhang, C. Li, Y. Shen and H. Uyama, *Small*, 2021, **17**, 2102160.
15. J. Zhang, X. Xu, L. Yang, D. Cheng, and D. Cao, *Small Methods*, 2019, **3**, 1900653.
16. L. Guo, F. Luo, F.i Guo, Q. Zhang, K. Qu, Z. Yang and W. Cai, *Chem. Commun.*, 2019, **55**, 7623-7626.
17. X. Mu, J. Gu, F. Feng, Z. Xiao, C. Chen, S. Liu and S. Mu, *Adv. Sci.*, 2021, **8**, 2002341.
18. B. Sarkar, D. Das and K. K. Nanda, *J. Mater. Chem. A*, 2021, **9**, 13958–13966.
19. F. Zhang, Y. Zhu, Y. Chen, Y. Lu, Q. Lin, L. Zhang, S. Tao, X. Zhang and H. Wang, *J. Mater. Chem. A*, 2020, **8**, 12810-12820.
20. S. Okazoe, K. Kusada, D. Wu, T. Yamamoto, T. Toriyama, S. Matsumura, S. Kawaguchi, Y. Kubotae and H. Kitagawa, *Chem. Commun.*, 2020, **56**, 14475-14478.
21. J. Chen, C. Chen, Y. Chen, H. Wang, S. Mao and Y. Wang, J. Catal., 2020, 392, 313-321.
22. Y. Zheng, Y. Jiao, Y. Zhu, L. H. Li, Y. Han, Y. Chen, M. Jaroniec and S.-Z. Qiao, *J. Am. Chem. Soc.*, 2016, **138**, 16174-16181.
23. Y. Wang, Q. Zhu, T. Xie, Y. Peng, S. Liu and J. Wang, *ChemElectroChem*, 2020, **7**, 1182-1186.
24. X. Wu, Z. Wang, D. Zhang, Y. Qin, M. Wang, Y. Han, T. Zhan, B. Yang, S. Li, J. Lai and L. Wang, *Nat. Commun.*, 2021, **12**, 4018.
25. J.-Y. Han, S.-H. Cai, J.-Y. Zhu, S. Yang and J.-S. Li, *Chem. Commun.*, 2022, **58**, 100-103.
26. Z. Liu, X. Yang, G. Hu and L. Feng, *ACS Sustainable Chem. Eng.*, 2020, **8**, 9136-9144.